Biosensors and Bioelectronics 79 (2016) 685–692

Contents lists available at ScienceDirect

Biosensors and Bioelectronics

journal homepage: www.elsevier.com/locate/bios

Electrochemical and bio-sensing platform based on a novel 3D Cu nano-flowers/layered MoS_2 composite

Xiaoyun Lin [a,**], Yongnian Ni [b,*], Serge Kokot [c]

[a] College of Chemistry, Nanchang University, Nanchang 330031, China
[b] State Key Laboratory of Food Science and Technology, Nanchang University, Nanchang 330047, China
[c] School of Chemistry, Physics and Mechanical Engineering, Queensland University of Technology, Brisbane 4001, Australia

ARTICLE INFO

Article history:
Received 10 September 2015
Received in revised form
4 December 2015
Accepted 20 December 2015
Available online 30 December 2015

Keywords:
Biosensor
Molybdenum disulfide
3D Cu nanoflowers
Hydrogen peroxide
Glucose

ABSTRACT

A novel 3D nano-flower-like Cu/multi-layer molybdenum disulfide composite (CuNFs/MoS_2) modified glassy carbon electrode (GCE) has been successfully constructed. It was a highly sensitive and selective non-enzymatic hydrogen peroxide (H_2O_2) and glucose biosensor. The morphology of the obtained CuNFs-MoS_2 nano-particles was investigated with the use of a scanning electron microscopy (SEM), transmission electron microscopy (TEM), X-ray diffraction (XRD) and energy dispersive X-ray spectroscopy (EDS). The physicochemical properties of the modified electrode were characterized at each of the construction stages with the use of an electrochemical impedance spectroscopy (EIS) and cyclic voltammetry (CV) techniques. The new sensor combined the advantages of MoS_2 and CuNFs, and exhibited high electro-catalytic activity toward H_2O_2 and glucose. Quantitative analysis of H_2O_2 and glucose was carried out with the use of the amperometric *i–t* method. Linear ranges were obtained between 0.04–1.88 μM and 1.88–35.6 μM for H_2O_2 and 1–20 μM and 20–70 μM for glucose, and their corresponding limits of detection (LOD) were 0.021 μM and 0.32 μM. This novel sensor was successfully applied for the quantitative analysis of H_2O_2 in tap water and glucose in human serum samples.

1. Introduction

Electrochemical sensors are generally considered as the most convenient and effective tools for hydrogen peroxide (H_2O_2) and glucose analysis to date, because they exhibit many attractive features, such as excellent sensitivity, time efficiency, simple instrumentation, easy operation, and low production cost. Based on the electrochemical method, horseradish peroxidase and glucose oxidase sensors have been most studied. However, compared with the non-enzymatic sensor, the activity of the enzyme is susceptible to environmental temperature, pH value, humidity, and toxic chemicals (Wilson and Turner, 1992; Qiang et al., 2011; Huang et al., 2014; Wang et al., 2014a, 2014b). The use of enzymes is usually cost-effective, and enzyme-based sensing requires either non-physiological electron mediators or oxygen. Thus, non-enzymatic sensors, especially those based on nanocomposites, seem to be the greatest interest to scientists involved in sensor and biosensors studies (Huang et al., 2014; Wang et al., 2014a, 2014b).

In general, materials with two-dimensional (2D) layers are often investigated for use in future electronic devices; in this context, some recent research has been focused on unusual morphologies of molybdenum disulfide (MoS_2). MoS_2 has a sandwich structure of three hexagonal atomic layers (S–Mo–S). Strong covalent bonding among atoms enables the formation of 2D layers, with the layers loosely bound to each other via weak van der Waals interactions. The anisotropic structure of MoS_2 leads to significant anisotropy in electrical conductivity (Late et al., 2012, 2014). The layered MoS_2 crystals generally offer very high electronic performance in a top gate structure with highly desirable on-off ratios, which are comparable to those of graphene nanoribbons. Also, these structural analogs of graphene potentially promise ultra-high sensitivities for the determination of environmental and biological molecules because they have high surface-to-volume ratios (Lee et al., 2011; Ayari et al., 2007; Radisavljevic et al., 2011; Lee et al., 2013). Furthermore, the layered MoS_2 allows ionic or molecular intercalation, and this may lead to possible applications in ion batteries (Mortazavi et al., 2014; Liu et al., 2014; Wang et al., 2014d), hydrogen storage (Chen et al., 2001; Ye et al., 2006; Putungan et al., 2015), catalysis (Lukowski et al., 2013; Cuddy et al., 2014), electrochemical double-layer capacitors (Zhao et al., 2013) and electrochemical sensors (Wang et al., 2013b, 2014c, 2015b).

For metal nanoparticles, shapes, sizes and compositions can effectively tune their properties by exposing different lattice planes

* Corresponding author.
** Corresponding author.
E-mail addresses: ynni@ncu.edu.cn (Y. Ni), s.kokot@qut.edu.au (S. Kokot).

http://dx.doi.org/10.1016/j.bios.2015.12.072
0956-5663/

and thus, providing different numbers of active sites (Lu and Chen, 2012). Thus, in the development and investigation of metal nanoparticles, it is very important to synthesize them under different experimental conditions so as to compare their properties.

In this work, Cu nanoflowers (CuNFs) were electrodeposited from a solution of 1.0×10^{-3} mol L^{-1} $Cu(NO_3)_2$ containing 0.1 mol L^{-1} Na_2SO_4 and 0.01 mol L^{-1} HNO_3 (Lin et al., 2014). Copper-based catalysts or catalyst promoters are of considerable general interest because of their wide range of applications in a variety of industrial processes (Jia et al., 2014), e.g. the CO_2 reduction activities of modified Cu electrode exhibited a strong dependence on the initial thickness of the Cu_2O layer (Li and Kanan, 2012).

It has been demonstrated in the literature that a mono-layer of MoS_2, which has been doped with Cu_4 clusters is very successful oxidation of CO; in particular, this process has low costs and produces a system with high activity (Chen et al., 2015).

Any sulfur on the surface of MoS_2 can interact with metals, including copper nano-particles (CuNPs). The bond between MoS_2 and the copper nano-structures was found to be well performing catalyst for small molecules (Zhong et al., 2012a; Chen et al., 2012; Gutierrez et al., 2013). In this case, the specific surface is considerably increased when MoS_2 combines with Cu; the resulting structure effectively is able to support a large number of electroactive species, and it significantly facilitates mass and electron transfer.

The aims of this investigation were: 1. to use of a layer-by-layer construction method so as to produce stable mixed films of 3D nano-flower-like Cu/layered MoS_2 composite, 2. to investigate the electrochemical and electrocatalytic performance of the CuNFs-MoS_2/GCE (GCE, glassy carbon electrode) with the use of the cyclic voltammetry and amperometric methods, and 3. to research and develop a quantitative electroanalytical method for the analysis of H_2O_2 and glucose at the CuNFs-MoS_2/GCE with the use of the amperometric *i-t* technique.

2. Experimental

2.1. Reagents

Glucose (A.R.), copper (II) nitrate trihydrate ($Cu(NO_3)_2\cdot3H_2O$, A.R.) and molybdenum sulfide (MoS_2, 99.5% metals <2 μm) were obtained from Aladdin Chemistry Co., Ltd., Shanghai, China. All other chemicals (A.R.) were obtained from Beijing Chemical Reagent Co., China and used without further purification. Phosphate buffer solution (PBS, pH 7.0, 0.1 M, prepared from KH_2PO_4 and Na_2HPO_4) was used as the supporting electrolyte; the pH of the buffer was monitored with an Orion SA720 digital pH meter (Orion Research Inc., Boston, MA, USA). Double-distilled water was used throughout the experiments.

2.2. Instrumentation

Electrochemical experiments were performed with the use of a CHI660A electrochemical workstation (Chenhua Apparatus Co., Shanghai, China) in conjunction with a three-electrode system: the working electrode – a modified GCE (3 mm diameter), the counter electrode-a platinum wire, and the reference saturated calomel electrode (SCE). Electrode potentials were measured with respect to the SCE. A cell stand (Model BAS C1A, USA) was used for voltammetric scanning and to stir the testing solution during the pre-concentration step.

Scanning electron microscopy (SEM) images were obtained using the Quanta 200F instrument (FEI Ltd., Tokyo, Japan). The samples were electro-deposited or dropped onto the detachable GCE. The power level was 20 kV.

Transmission electron microscopy (TEM) and energy dispersive X-ray spectroscopy (EDS) were carried out with the use of a JEM-2010 (JEOL Co., Japan) in order to measure the structure and morphology of the obtained compounds; the associated point and linear resolutions were found to be 0.23 nm and 0.14 nm, respectively. The accelerating voltage was set at 200 kV. A given sample was placed on a carbon-coated copper grid by depositing a drop of the test solution on the grid. The deposited sample was dried in air at room temperature.

X-ray diffraction data were recorded with the use of a Bede D1 System (Bede Scientific Instruments, Durham, UK) using Cu K_α radiation ($\lambda=1.5406$) and a Bragg angle range of 10–80°.

2.3. Preparation of MoS_2

MoS_2 (100 mg) was placed into a 250 mL beaker and N,N-dimethylformamide (DMF) (100 mL) was added. The mixture was ultrasonicated by a KQ-500DE sonicater (Kunshan ultrasonic instrument Co., China) at room temperature (22 ± 2 °C) for 4 h, and a black suspension formed. After standing for 24 h at room temperature (22 ± 2 °C), the supernatant layer was then transferred to the centrifuge tubes, and centrifuged at 12,000 rpm for 30 min; the separated solid separed and collected (Wang et al., 2013b).

2.4. Preparation of CuNFs-MoS_2/GCE

Glassy carbon electrodes (GCE, 3 mm) were polished with emery paper and alumina slurry; they were then successively rinsed with dilute nitric acid, ethanol, and distilled water in an ultrasonic bath. Thereafter, the electrodes were immersed in 0.25 mol L^{-1} H_2SO_4 and the potential at the electrodes was changed in the -1.0 and 1.0 V range until a steady potential was obtained.

MoS_2 nanoparticles were dispersed in DMF (approximately 1.0 mg mL^{-1} solution). Then 15 μL of this suspension was deposited on the surface of the GCE. The solvent was allowed to evaporate to dryness in air and the MoS_2 nanoparticles then formed very stable films even without the protection of Nafion or chitosan. In the following experiments the surface of the MoS_2/GCE was rinsed with redistilled deionized water to avoid any possible effects of residual DMF.

The MoS_2/GCE was immersed in 1.0×10^{-3} mol L^{-1} $Cu(NO_3)_2$ solution containing 0.1 mol L^{-1} Na_2SO_4 and 0.01 mol L^{-1} HNO_3. The solution was electrolysed at -0.35 V (vs. SCE) for 60 s and the CuNFs were then electrodeposited on the MoS_2/GCE (Scheme 1). The result showed the best catalytic performance for hydrogen peroxide (H_2O_2) and glucose biosensor after 60 s deposition time (Fig. S1, Supplementary Material). Finally, the obtained electrode, CuNFs-MoS_2/GCE, was rinsed three times with twice-distilled water. The other electrode, CuNFs/GCE, was prepared following the same procedure.

3. Results and discussion

3.1. Characterization of the CuNFs-MoS_2 composite

It has been demonstrated that ultra-sonication was an easy and efficient approach for the exfoliation of graphite, bulk MoS_2, and other layered materials into a single layer (Choucair et al., 2009). MoS_2 nano-particles could be readily obtained in a narrow size distribution by processing them with the use of ultra-sonication

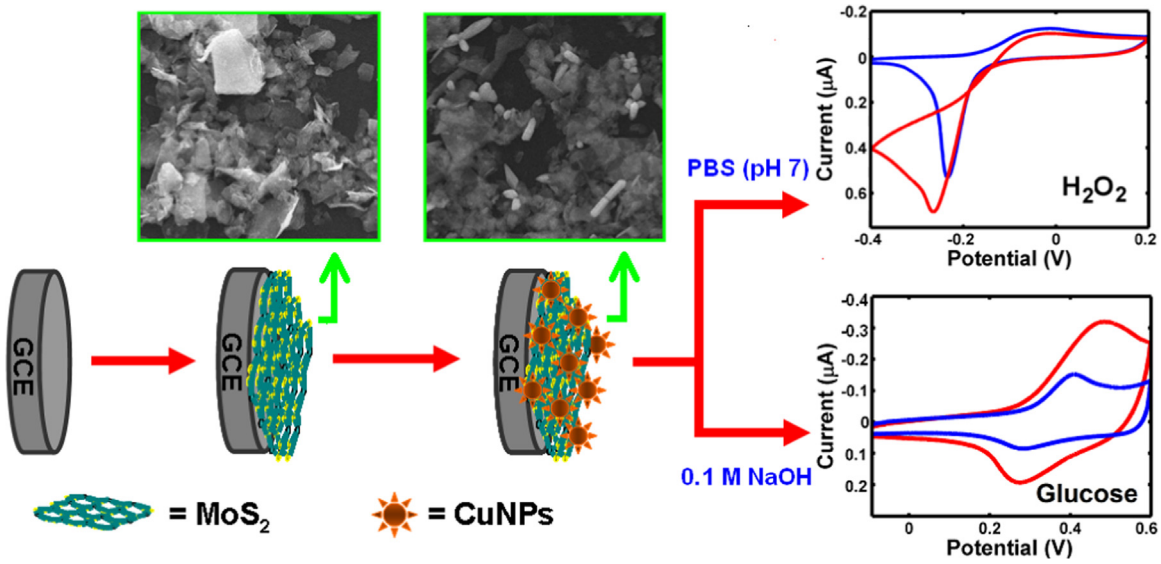

Scheme 1. A schematic representation of the fabrication of the CuNFs-MoS_2/GCE, and possible reaction mechanisms at the electrode during the analysis for H_2O_2 and glucose.

and gradient centrifugation techniques. The transmission electron microscopy (TEM) image (Fig. 1A) was taken from some the prepared MoS_2 nano-particles. It shows that different MoS_2 layers can be folded and tangled so as to form a multilayered morphology. Energy-dispersive X-ray spectrum (EDS) analysis was performed to characterize the chemical composition of MoS_2 (Fig. 1B) and to confirm the presence of the elements: Mo, S and Cu.

The morphologies of the MoS_2/GCE (Fig. 1C), CuNFs/GCE (Fig. 1D and E) and CuNFs-MoS_2/GCE (Fig. 1F) were investigated with the use of the scanning electron microscopy (SEM technique). Thus, there were flake-like MoS_2 particles distributed homogeneously on the GCE (Fig. 1C), and Fig. 1D and E demonstrate that Cu nano-flowers uniformly covered the GCE. These particles demonstrated the presence of an unusual three-dimensional structure consisting of crystals each with a five petal – like form. When Cu was electro-deposited on the surface of the MoS_2/GCE, flake-like MoS_2 aggregates became smaller and smaller and simultaneously, 3D CuNFs were deposited on MoS_2 (Fig. 1F).

The X-ray powder diffraction (XRD) pattern of the CuNFs, MoS_2 and CuNFs-MoS_2 composites are presented in Fig. 1G. The diffraction pattern of the substrate (GCE) indicates typical broad and weak reflections located in the range of 16-38°. The XRD pattern of CuNFs-MoS_2 have peaks at approximately 43.5°, 50.5° and 74.3°, which can be assigned to Cu (111), Cu (200) and Cu (220), respectively (Zhao et al., 2015); also, peaks at approximately 14°, 39°, 44°, 50° and 60° suggested the presence of the MoS_2 (002), (103), (104), (105) and (112) (Wang et al., 2013a; Chang and Chen, 2011). These observations confirmed that the CuNFs-MoS_2 composite has been prepared successfully.

3.2. Electrochemical properties of the CuNFs-MoS_2/GCE

Electrochemical properties of the CuNFs-MoS_2/GCE were investigated with the use of the electrochemical impedance spectroscopy (EIS), cyclic voltammetrys (CVs) and chronocoulometry (Fig. 2). The electrolyte consisted of 5×10^{-3} mol L^{-1} $[Fe(CN)_6]^{3-/4-}$ (1:1) in 0.1 mol L^{-1} KCl.

The EIS Z′ (real part) *versus* Z″(imaginary part) of the impedance graph indicated that the electron-transfer resistance (R_{et}) at the electrode surface was the same as the diameter of the semi-circle on the Nyquist plot; thus, this graph can be used to describe the properties at the interface of the electrode (Lin et al., 2015). Significant response differences between such semicircular diameters, R_{et}, on the Z′ *versus* Z″profiles were observed as a function of the stepwise modification of the working electrode, i.e. from its GCE state to the fully modified CuNFs-MoS_2/GCE (Fig. 2A). The response profile for the untreated GCE (curve a, Fig. 2A) was effectively a straight line; this indicated the presence of a small impedance at the interface. When the CuNFs were electro-deposited on the surface of the GCE, the impedance values (R_{et}) did not show any significant changes compared with the behavior at the GCE (b, Fig. 2A). This indicated that the CuNFs/GCE was a strongly conducting electrode. When the MoS_2 were deposited on the GCE surface, the impedance curve of the MoS_2/GCE indicated the presence of a relatively well formed semi-circle (c, Fig. 2A). This demonstrated the presence of a relatively high electron transfer resistance and suggested that the MoS_2/GCE had poor conductivity. However, when the fully modified CuNFs-MoS_2/GCE (d, Fig. 2A) was tested, the impedance curve of the modified electrode was further reduced as compared to that from the MoS_2/GCE. Thus, this observation suggested that CuNFs was immobilized on the MoS_2/GCE film.

CV experiments with the same electrode systems and condition (Fig. 2B) gave a similar conclusion obtained from the EIS work above, i.e. the untreated GCE exhibited two well defined redox peaks (curve a, Fig. 2B). After electrodeposition of CuNFs, the current value did not show any significant changes compared with that observed with the GCE; this may be attributed to the good electrical conductivity of the CuNFs, (b, Fig. 2B). Then, when nano-MoS_2 was modified on the GCE, the redox peak current decreased, as expected, because it is well known that the conductivity of nano-MoS_2 is poor, (c, Fig. 2B). Following these observations, when the CuNFs-MoS_2/GCE was tested, the current values increased further as compared to those from the MoS_2/GCE (d, Fig. 2B).

Chronocoulometric results obtained from the reduction of 5×10^{-3} mol L^{-1} $K_3[Fe(CN)_6]$ in KCl (0.1 mol L^{-1} at different electrodes, were used to compare the apparent electrode areas with the use of Eq. (1) (Song et al., 2014):

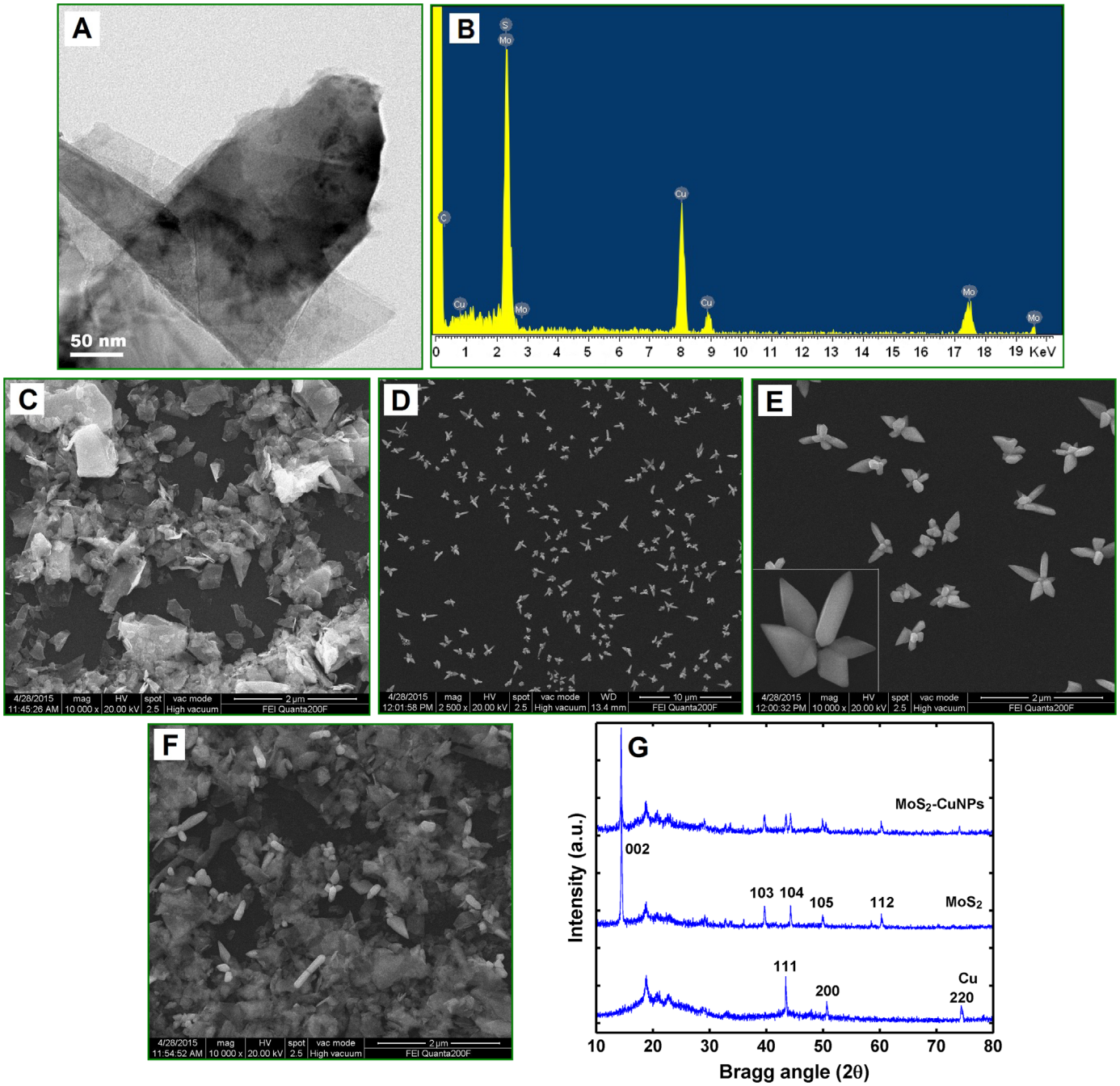

Fig. 1. (**A**) TEM image of MoS_2. (**B**) EDS of MoS_2. (**C**) SEM image of MoS_2/GCE. (**D**) and (**E**) SEM images of CuNFs/GCE with different scales (inset in E: amplified SEM of CuNFs). (**F**) SEM image of CuNFs-MoS_2/GCE. (**G**) XRD patterns of of CuNFs/GCE, MoS_2/GCE and CuNFs-MoS_2/GCE.

$$Q = (2nFAD_0^{1/2}\Pi^{-1/2}C_0)t^{1/2} \quad (1)$$

where *Q*-the absolute value of the reduction charge, *n* – the number of electrons transferred, *F*-the Faraday constant, *A*-the apparent electrode area, *t*- the time, and D_0 and C_0-the diffusion coefficient and the bulk concentration of the oxidized form of the hexacyanoferrate (III) complex, respectively.

The apparent electrode area, *A*, may be estimated from the slope of the *Q versus* $t^{1/2}$ plot (Fig. 2C). Thus, the order of the slope values was: CuNFs-MoS_2/GCE(d) > CuNFs/GCE(b) > MoS_2/GCE(c) > GCE(a), i.e. CuNFs-MoS_2/GCE has the largest *A* value, and thus, this modified electrode showed the best electrochemical activity.

3.3. Electrochemistry and electrocatalysis of the CuNFs-MoS_2/GCE toward H_2O_2

In biological and environmental processes, H_2O_2 is often an important intermediate species, and therefore, its analysis is of practical importance (Wang et al., 2014a). The experimental conditions were optimized to obtain the best sensitivity. The pH 7.0 and operational potential of -0.30 V (see Fig. S2, Supplementary Material) were chosen for subsequent amperometric measurements for H_2O_2.

The CVs of the CuNFs-MoS_2/GCE in 0.1 M PBS (pH 7.0) have different scan rates from 0.02 to 0.30 V s^{-1} (Fig. 3A), and the redox peak currents increased linearly with the square root of the scan rate (inset, Fig. 3A). This suggested that diffusion controlled processes

were present. This was well demonstrated by the CVs collected at the CuNFs-MoS_2/GCE in 0.1 M PBS (pH 7.0) in the absence (curve a) and presence (curve b) of 2.0 μM H_2O_2, and it was quite evident that the reduction peak current significantly increased in the presence of H_2O_2. The results indicated that the above modified electrode responds particularly for the analysis of H_2O_2.

Amperometric experiments were carried out at three differently modified electrodes: MoS_2/GCE, CuNFs/GCE and CuNFs-MoS_2/GCE, which were immersed in 0.1 M pH 7.0 PBS containing 0.04–0.44 μ mol L^{-1} H_2O_2 (Fig. 3C). In this case, the solution was stirred and saturated with nitrogen gas (). The results indicated that MoS_2/GCE did catalyse H_2O_2 (curve a, Fig. 3C), but a much larger catalytic current was recorded at the CuNFs/GCE (curve b, Fig. 3C). However, the largest current was observed at the electrode constructed from MoS_2 and CuNFs (curve c, Fig. 3C). This significant improvement can be attributed to the synergistic, catalytic effect of MoS_2 and CuNFs. Also, this observation can be explained by noting that the CuNFs-MoS_2/GCE has a larger surface area, and thus, is able to adsorb more H_2O_2 molecules. According the literature (Wang et al., 2015a), the possible reaction process could be expressed as: (1) with the presence of H_2O_2, MoS_2 nanosheets were oxidized to MoS_2OH; (2) HOO· produced by the reaction of H_2O_2 and ·OH; (3) O_2 was produced due to MoS_2OH and HOO·.

$$H_2O_2 + MoS_2 \rightarrow HO + MoS_2OH \quad (2)$$

$$H_2O_2 + HO \rightarrow HOO + H_2O \quad (3)$$

$$MoS_2OH + HOO \rightarrow H_2O + O_2 + MoS_2 \quad (4)$$

Amperometric response of the CuNFs-MoS_2/GCE toward H_2O_2 under optimal conditions was demonstrated in Fig. 3E. The current response increased steadily with the addition of H_2O_2 in the range of 0.04–1.88 μM and 1.88–35.6 μM; the LOD was 0.021 μM (inset, Fig. 3F). Compared to some earlier sensors, which were based on Cu nanoparticles modified electrode, the sensor, CuNFs-MoS_2/GCE, investigate in this work, demonstrated superior sensitivity (see Table S1, Supplementary Material).

3.4. Electrochemistry and electrocatalysis of the CuNFs-MoS_2/GCE toward glucose

Experimental conditions for analysis of glucose were optimized, and 0.1 M NaOH was chosen as the supporting electrolyte and +0.50 V as the operational potential (see Fig. S3, Supplementary Material).

The CVs of the CuNFs-MoS_2/GCE in 0.1 M NaOH were collected in the presence of glucose in the 0.02–0.26 V s^{-1} scan range (Fig. 4A). The redox peak currents increased linearly with the square root of scan rate (inset, Fig. 4A), in a manner similar to that observed with the H_2O_2 analyte. It would appear that diffusion controlled process could be responsible for the above observations. Similarly to previous work (Wang et al., 2014a; Toghill and Compton, 2010), the electrochemical reactions for glucose were most likely to be:

$$Cu(0) + 2OH^- \rightarrow Cu(OH)_2 + 2e^- \quad (5)$$

$$Cu(OH)_2 + OH^- \rightarrow CuOOH + H_2O + e^- \quad (6)$$

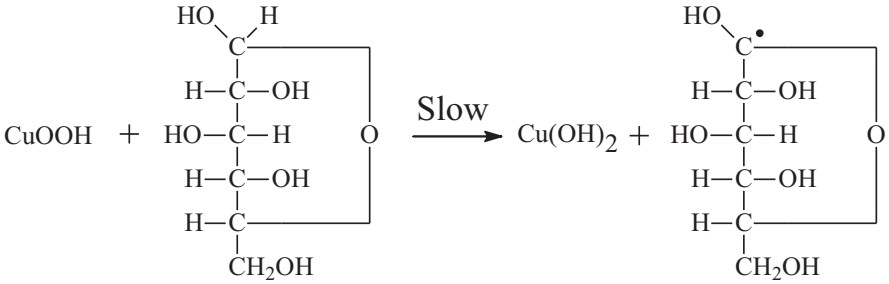

(7)

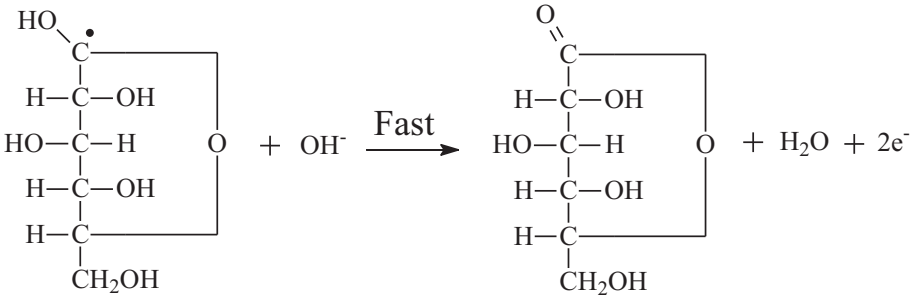

(8)

Selectivity of the CuNFs-MoS_2/GCE was investigated under the same conditions described above, and in the presence of some common substances, such as dopamine (DA), ascorbic acid (AA), urea (UA), fructose, lactose and galactose. The plot of current *versus* potential (Fig. 3D) clearly indicated that these compounds produce little interference for the analysis of H_2O_2.

In 0.1 M NaOH solution, the CuNFs can easily transform into $Cu(OH)_2$, and then under high potential conditions, the $Cu(OH)_2$ can be further oxidized to generate a large number of CuOOH species, which can oxidize glucose to gluconolactone.

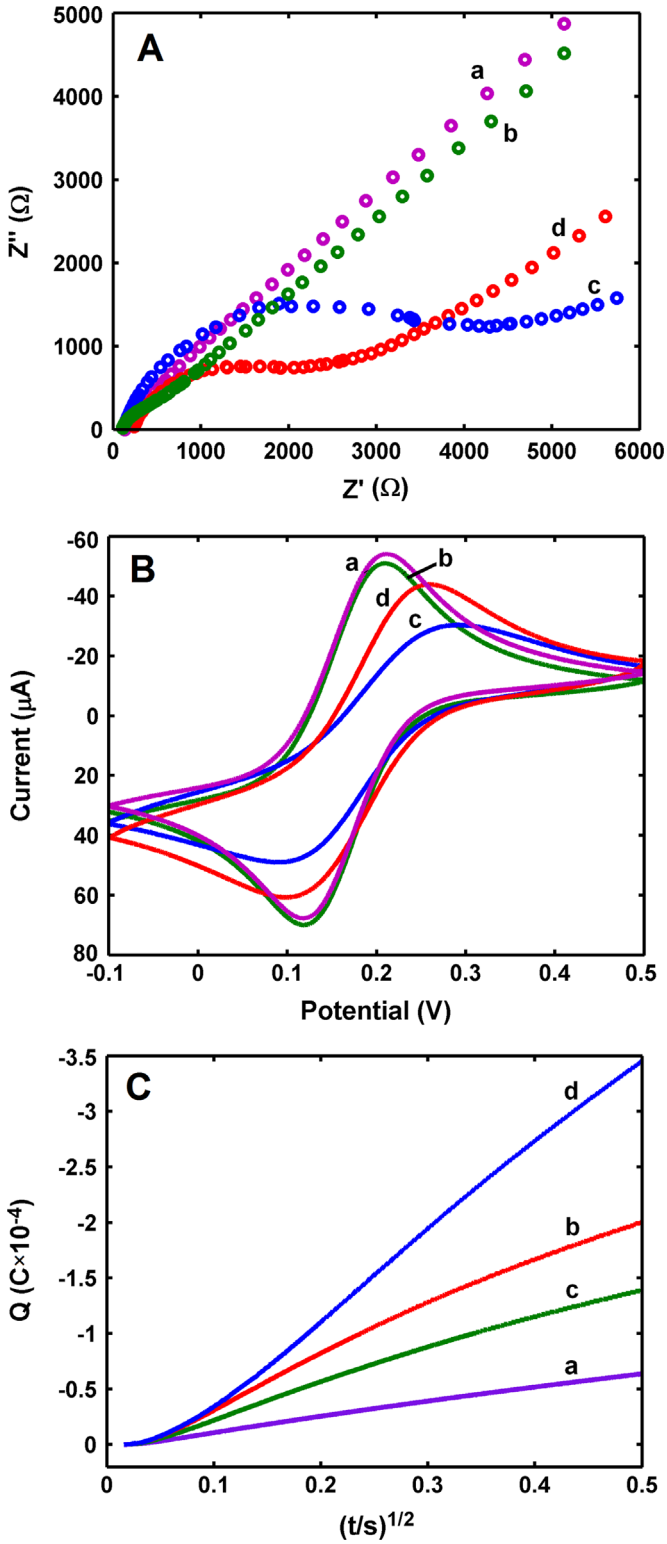

Fig. 2. (**A**) Electrochemical impedance spectroscopy (EIS). (B) cyclic voltammogram (CV) and (C) chronocoulometric plots from: (**a**) GCE, (**b**) CuNFs/GCE, (**c**) MoS_2/GCE, and (**d**) CuNFs-MoS_2/GCE, in 5×10^{-3} mol L^{-1} $[Fe(CN)_6]^{3-/4-}$ (1:1) solution containing 0.1 M KCl.

The CVs of the CuNFs-MoS_2/GCE in 0.1 M NaOH without (curve a) and with (curve b) 0.1 mM glucose at 50 mV s^{-1} are shown in Fig. 4B. Interpretation of these results strongly suggested that the peak current increased substantially on addition of 20 μM glucose, and this indicated that catalytic oxidation readily occurred at the electrode in the presence of glucose. The amperometric response of the differently modified electrodes, MoS_2/GCE, CuNFs/GCE and CuNFs-MoS_2/GCE, toward glucose in 0.1 M NaOH containing 1–20 μM glucose was demonstrated in Fig. 4C. It was shown that MoS_2/GCE cannot catalyse the glucose (curve a, Fig. 4C), but a catalytic current was clearly present at the CuNFs/GCE (b, Fig. 4C). A larger catalytic current was observed (curve c) when MoS_2 was combined with CuNFs. Maybe CuNFs on the MoS_2 substrate have good catalytic properties to glucose.

Various possible interfering substances, such as DA, AA, UA, fructose, lactose and galactose, were used (supporting electrolyte: 0.1 M NaOH; applied potential: +0.5 V) to investigate the method selectivity. The results showed that the interfering species (0.1 mM for each analyte) did not significantly influence the determination of glucose (see Fig. 4D). The plot of response current at the CuNFs-MoS_2/GCE *versus* glucose concentration (Fig. 4E) was linear in the 1–20 μM and 20–70 μM range, with an LOD of 0.32 μM (inset, Fig. 4F). The results compared well with those previously published electrochemical methods based on copper nanoparticles (Table S2, Supplementary Material).

3.5. Reproducibility and stability

To investigate the reproducibility and stability of the modified electrode, CuNFs-MoS_2/GCE, this sensor was prepared separately five times with the use of the same GCE. H_2O_2 (2.0 μM) and glucose (20 μM) were tested respectively, and their relative standard deviations (%RSD) of the measurements were 3.74% and 4.68%, respectively. The stability of the sensor was estimated by detecting 2.0 μM H_2O_2 and 20 μM glucose after it was stored at 4 °C for two weeks; repeat analyses showed that the current intensity for H_2O_2 and glucose decreased only by 2.78% and 3.57%, respectively. The results indicated that the CuNFs-MoS_2/GCE was stable and repeatable, and thus, it can be used for detection H_2O_2 and glucose selectively.

3.6. Analytical applications

The biosensor was applied to detect the H_2O_2 in tap water and the glucose in human serum. Before the measurements, the tap water samples were 5-fold diluted with 0.01 M PBS (pH=7.0) (nitrogen saturated solution) and the blood samples were 20-fold diluted with 0.1 M NaOH. Each tap water or blood sample was spiked with standard H_2O_2 or glucose solutions (Zhong et al., 2012b). Then the proposed method was applied and the corresponding results (Table 1) showed that the biosensor gave quite acceptable recoveries, which indicated that the proposed electrode may have a potential for practical application.

4. Conclusions

A highly sensitive and selective non-enzymatic biosensor, CuNFs-MoS_2/GCE, has been successfully constructed to analyse H_2O_2 and glucose at low concentration levels. The biosensor sensitivity and stability can be attributed to the synergistic, catalytic effects of the CuNFs and MoS_2. Because such structure provides a large specific surface area, it effectively supports a large number of electroactive species, and thus, considerably enhances the mass and electron transfer. To demonstrate practical applications of this biosensor, it was applied to analyse quantitatively H_2O_2 in tap water and glucose in human serum samples. These analysis were successful as were the recovery trials; the results for the two analytes were between 97.3-106%. Importantly, these results also showed that the CuNFs-MoS_2/GCE was an effective sensing platform for small biological molecules.

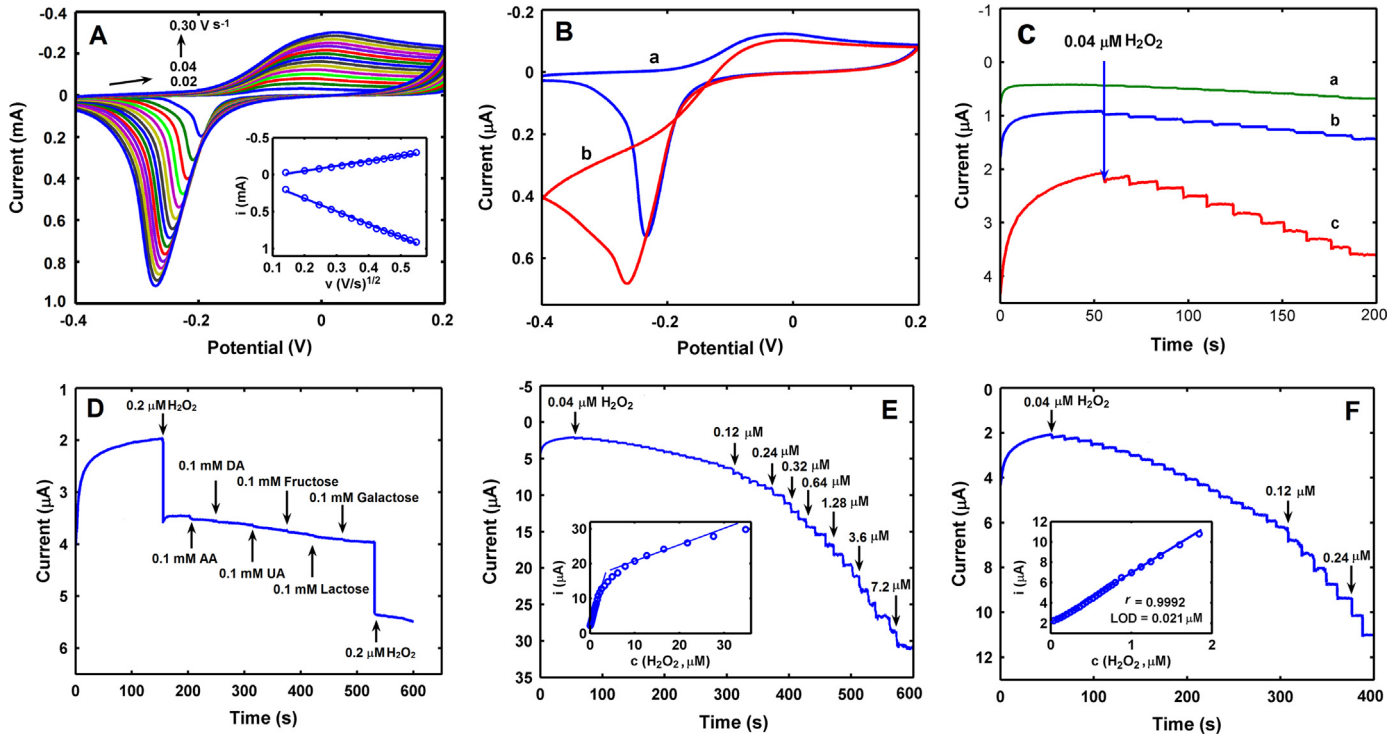

Fig. 3. (**A**) CVs of the CuNFs-MoS_2/GCE in 0.1 M PBS (pH 7.0) at various scan rates. **Inset**: plot of peak current *versus* square root of scan rates. (**B**) CVs of the CuNFs-MoS_2/GCE in the (**a**) absence and (**b**) presence of 2.0 μM H_2O_2 in 0.1 M pH 7.0 PBS at 0.10 V s^{-1}. (**C**) Amperometric response recorded at: (**a**) the MoS_2/GCE, (**b**) CuNFs/GCE and (**c**) CuNFs-MoS_2/GCE, after successive additions of H_2O_2 to 0.1 M PBS (pH 7.0) at −0.30 V. (**D**) Amperometric response of the CuNFs-MoS_2/GCE to different chemicals at −0.30 V. (**E**) and (**F**) Amperometric response of the CuNFs-MoS_2/GCE after successive addition of H_2O_2 to 0.1 M PBS (pH 7.0) at −0.30 V. **Inset**: calibration plot.

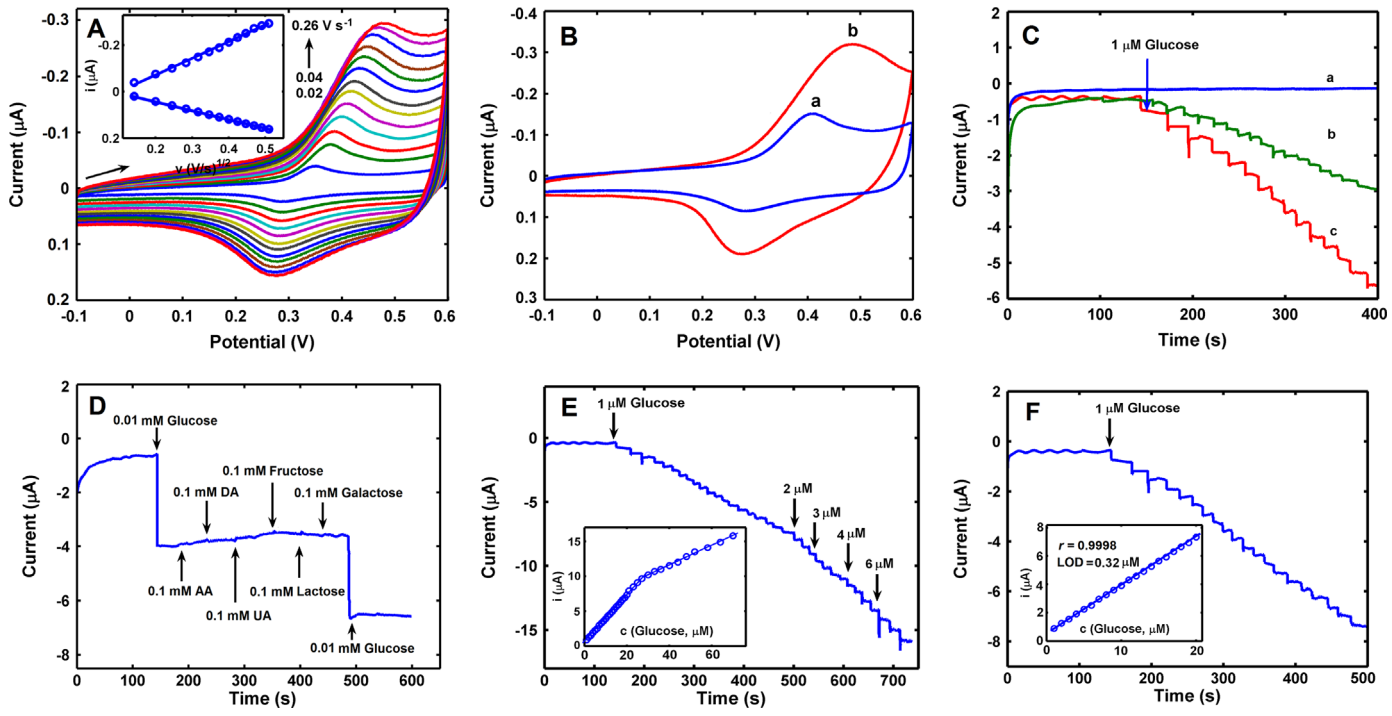

Fig. 4. (**A**) CVs of the CuNFs-MoS_2/GCE in 0.1 M NaOH at various scan rates. **Inset**: plot of peak current *versus* square root of scan rates. (**B**) CVs of the CuNFs-MoS_2/GCE in the (**a**) absence and (**b**) presence of 20 μM glucose in 0.1 M NaOH at 0.10 V s^{-1}. (**C**) Amperometric response recorded at: (**a**) the MoS_2/GCE, (**b**) CuNFs/GCE, and (**c**) CuNFs-MoS_2/GCE, upon successive addition of glucose to 0.1 M NaOH at +0.50 V. (**D**) Amperometric response of the CuNFs-MoS_2/GCE to different chemicals at +0.50 V. (**E**) and (**F**) Amperometric response of the CuNFs-MoS_2/GCE after successive additions of glucose to 0.1 M NaOH at +0.50 V. **Inset**: the calibration plot.

Table 1
Results of the quantitative analyses of H_2O_2 in tap water and glucose in human serum.

Samples	Content (μM)	RSD (%) [a]	Added (μM)	Detected (μM)	%Recovery [b]
Tap water					
#1	0.5	4.2	0.5	1.03	106.0
#2	1.0	3.6	0.5	1.48	98.0
#3	1.5	3.1	0.5	1.96	97.3
Human serum					
#1	5.0	3.2	5.0	10.1	102.0
#2	10.0	3.5	5.0	15.3	103.0
#3	15.0	2.6	5.0	19.8	98.7

[a] RSD (%) calculated from three separate experiments.
[b] % Recovery $= 100 \times (c_{detected} - c_{added})/c$

Acknowledgments

The authors gratefully acknowledge the financial support of this study by the National Natural Science Foundation of China (NSFC-31401587), the Natural Science Foundation of Jiangxi Province (20142BAB213009), and the State Key Laboratory of Food Science and Technology of Nanchang University (SKLFZ-ZA201302 and SKLF-ZZB201303).

Appendix A. Supplementary material

Supplementary data associated with this article can be found in the online version at http://dx.doi.org/10.1016/j.bios.2015.12.072.

References

Ayari, A., Cobas, E., Ogundadegbe, O., Fuhrer, M.S., 2007. J. Appl. Phys. 101 (1–5), 014507.
Chang, K., Chen, W.X., 2011. ACS Nano 5, 4720–4728.
Chen, J., Kuriyama, N., Yuan, H., Takeshita, H.T., Sakai, T., 2001. J. Am. Chem. Soc. 123, 11813–11814.
Chen, Y.Y., Dong, M., Wang, J.G., Jiao, H.J., 2012. J. Phys. Chem. C 116, 25368–25375.
Chen, Z.W., Yan, J.M., Zheng, W.T., Jiang, Q., 2015. Sci. Rep. 5, 11230.
Choucair, M., Thordarson, P., Stride, J.A., 2009. Nat. Nanotechnol. 4, 30–33.
Cuddy, M.J., Arkill, K.P., Wang, Z.W., Komsa, H.P., Krasheninnikov, A.V., Palmer, R.E., 2014. Nanoscale 6, 12463–12469.
Gutierrez, O.Y., Zhong, L.S., Zhu, Y.Z., Lercher, J.A., 2013. Chemcatchem 5, 3249–3259.
Huang, J.W., He, Y.Q., Jin, J., Li, Y.R., Dong, Z.P., Li, R., 2014. Electrochim. Acta 136, 41–46.
Jia, X.F., Yang, X.A., Li, J., Liab, D.Y., Wang, E.K., 2014. Chem. Commun. 50, 237–239.
Late, D.J., Liu, B., Matte, H.S.S.R., Dravid, V.P., Rao, C.N.R., 2012. ACS Nano 6, 5635–5641.
Lee, K., Gatensby, R., McEvoy, N., Hallam, T., Duesberg, G.S., 2013. Adv. Mater. 25, 6699–6702.
Lee, K., Kim, H.Y., Lotya, M., 2011. Adv. Mater. 23, 4178–4182.
Lei, B., Li, G.R., Gao, X.P., 2014. J. Mater. Chem. A 2, 3919–3925.
Li, C.W., Kanan, M.W., 2012. J. Am. Chem. Soc. 134, 7231–7234.
Lin, X.Y., Ni, Y.N., Kokot, S., 2015. Anal. Chim. Acta 867, 29–37.
Lin, X.Y., Ni, Y.N., Kokot, S., 2014. Electrochim. Acta 133, 484–491.
Liu, Y.C., Zhao, Y.P., Jiao, L.F., Chen, J., 2014. J. Mater. Chem. A 2 (32), 13109–13115.
Lukowski, M.A., Daniel, A.S., Meng, F., Forticaux, A., Li, L.S., Jin, S., 2013. J. Am. Chem. Soc. 135 (28), 10274–10277.
Lu, Y.Z., Chen, W., 2012. Chem. Soc. Rev. 41, 3594–3623.
Mortazavi, M., Wang, C., Deng, J.K., Shenoy, V.B., Medhekar, N.V., 2014. J. Power Sources 268, 279–286.
Putungan, D.B., Lin, S.H., Wei, C.M., Kuo, J.L., 2015. Phys. Chem. Chem. Phys. 17 (17), 11367–11374.
Qiang, L.L., Vaddiraju, S., Patel, D., Papadimitrakopoulos, F., 2011. Biosens. Bioelectron. 26, 3755–3760.
Radisavljevic, B., Radenovic, A., Brivio, J., Giacometti, V., Kis, A., 2011. Nat. Nanotechnol. 6 (3), 147–150.
Song, H.Y., Ni, Y.N., Kokot, S., 2014. Biosens. Bioelectron. 56, 137–143.
Toghill, K.E., Compton, R.G., 2010. Int. J. Electrochem. Sci. 5, 1246–1301.
Wang, D.Z., Wang, Z.P., Wang, C.L., Zhou, P., Wu, Z.Z., Liu, Z.H., 2013a. Electrochem. Commun. 34, 219–222.
Wang, L., Zhang, Q.Y., Chen, S.L., Xu, F.G., Chen, S.H., Jia, J.B., Tan, H.L., Hou, H.Q., Song, Y.H., 2014a. Anal. Chem. 86, 1414–1421.
Wang, T., Yu, Y.A., Tian, H.F., Hu, J.B., 2014b. Electroanalysis 26, 2693–2700.
Wang, T.Y., Zhu, H.C., Zhuo, J.Q., Zhu, Z.W., Papakonstantinou, P., Lubarsky, G., Lin, J., Li, M.X., 2013b. Anal. Chem. 85, 10289–10295.
Wang, T.Y., Zhu, R.Z., Zhuo, J.Q., Zhu, Z.W., Shao, Y.H., Li, M.X., 2014c. Anal. Chem. 86 (24), 12064–12069.
Wang, X., Chu, C.C., Shen, L., Deng, W.P., Yan, M., Ge, S.G., Yu, J.H., Song, X.R., 2015a. Sens. Actuators B 206, 30–36.
Wang, X.X., Nan, F.X., Zhao, J.L., Yang, T., Ge, T., Jiao, K., 2015b. Biosens. Bioelectron. 64, 386–391.
Wang, Y.X., Chou, S.L., Wexler, D., Liu, H.K., Dou, S.X., 2014d. Chem. -Eur. J. 20 (31), 9607–9612.
Wilson, R., Turner, A.P.F., 1992. Biosens. Bioelectron. 7, 165–185.
Ye, L.N., Wu, C.Z., Guo, W., Xie, Y., 2006. Chem. Commun. 45, 4738–4740.
Zhao, L.P., Wang, H.Y., Qi, L., 2013. J. Inorg. Mater. 28 (8), 831–835.
Zhao, S., Wang, T.T., Wang, L.L., Xu, S.K., 2015. J. Solid State Electrochem. 19, 831–839.
Zhong, X., Yang, H.D., Guo, S.J., Li, S.W., Gou, G.L., Niu, Z.Y., Dong, Z.P., Lei, Y.J., Jin, J., Li, R., Ma, J.T., 2012a. J. Mater. Chem. 22, 13925–13927.
Zhong, X., Yuan, R., Chai, Y.Q., 2012b. Chem. Commun. 48, 597–599.